A new robust modeling strategy for multi-component droplet heat and mass transfer in general ambient conditions

Fernando Luiz Sacomano Filho, Artur Carvalho Santos, Aymeric Vié, Carlos Krieger Guenther

A new robust modeling strategy for multi-component droplet heat and mass transfer in general ambient conditions

Fernando Luiz Sacomano Filho[a,*], Artur Carvalho Santos[b], Aymeric Vié[b], Guenther Carlos Krieger Filho[a]

[a]*Laboratory of Environmental and Thermal Engineering, Universidade de São Paulo, São Paulo, Brazil.*
[b]*Laboratoire EM2C, CNRS, CentraleSupelec, Université Paris-Saclay, Gif-sur-Yvette, France.*

Abstract

Liquid fuels applied to spray combustion processes are predominantly composed by a mixture of components. Following an injection process, multi-component liquid droplets are subject of heat and mass transfer processes in a multitude of atmosphere compositions, resulting in complex interaction processes. This example based on a spray combustion process summarizes the diversity of scenarios that a droplet may experience in a spray flow. Typically, available models in the literature have limitations to characterize such complex interactions. In view of this, the present work proposes a novel modeling strategy to account for such interactions in diverse scenarios grounded in a consistent computational approach. To accomplish this task, a new formulation is derived from general transport equations of the gas phase. The resulting model is validated by comparing numerical results with available experimental data. Herein, binary mixtures of liquids evaporating in diverse atmospheres are considered. In contrast to other reference approaches, the derived model demonstrates to overcome all tested scenarios, which includes severe atmosphere compositions and states. Additional effects could be observed regarding the different diffusivity among the participating species, which are not only perceived in mass transfer but also on heat transfer. A more comprehensive description of the different underlying phenomena relative to the spray combustion could be obtained with the proposed strategy.

Keywords: Droplet evaporation, Evaporation modeling, Multi-component droplets, Spray combustion, Differential diffusion, Ethanol

*Corresponding author
Email address: fernando.sacomano@usp.br (Fernando Luiz Sacomano Filho)

1. Introduction

When considering combustion processes of hydrophilic fuels, a challenging scenario emerges: droplet heat and mass transfer processes in atmospheres with high mass fractions of a liquid vapor species. Concretely, these conditions can be present for example during the interaction of hydrous ethanol droplets with combustion products, where high mass fractions of water vapor exist. Such a scenario imposes a quite challenging task to the heat and mass transfer modeling where evaporation and condensation processes may occur interchangeably. This is not limited to liquid hydrophilic fuels, as it may occur in any flow where liquid droplets interact with atmospheres composed of varying vapor mass fractions crossing their corresponding saturation values.

To handle phase change on such conditions, one of the most important physical phenomena is the vapor diffusion into the surrounding gas. For single-component droplets, many models have been derived and are canonically used for combustion applications [1–3]. For multi-component vaporization, less contributions can be found [4–7] and no model emerge as a reference. However, as already pointed out by Brenn et al. [4], there is a need for a realistic description of the heat and mass transfer processes across the phase interface in order to achieve a thorough description of multi-component droplet evaporation. Therefore, the derivation of reliable and computationally efficient models able to accurately represent the differential diffusion transport among species and energy is desired.

Focusing on recent related works, Tonini and Cossali [6] presented a comparative analysis between different approaches which may account for the differential diffusion effects of evaporating liquid droplets. Two models have been proposed: one is an analytical model that accounts for the inter-species mass diffusion in the gaseous mixture and the other is based on the single-component analogy. Additionally, a novel solution strategy is proposed for the model based on the detailed description of diffusion transport, which contrasts with that presented in [8]. In both [6] and [8], Fick's law is applied for diffusion, and energy considerations follow the formulation of Abramzon and Sirignano [9]. The differential diffusion is considered in [4] under the assumption that each species interacts singly as a binary mixture with the surrounding air, following the ideal gas approach. Results show a good agreement with experimental data obtained from acoustically-

levitated droplets. Recently, this model was applied in [7] to study the evaporation of ethanol/water droplets at different ambient conditions, including variations in relative air humidity. Ebrahimian and Habchi [5] present a multi-component approach based on the so-called Hirschfelder-Curtiss simplification (e.g. [10, 11]). The resulting method is based on an iterative procedure to solve the mass flow rate, droplet temperature, and composition of the liquid and gas mixtures. Presented results could well represent the trends observed experimentally for binary mixtures of n-heptane and n-decane. Focusing on binary mixtures of ethanol and water, Lupo and Duwig [12] performed numerical investigations of different initial droplet compositions and effects of preferential diffusion of liquid vapor into the surrounding gas. To address the effects of preferential diffusion, an approach is proposed to address the enthalpy fluxes caused by the different species specific heats into the gas energy equation. Despite the special attention given to ethanol and water binary mixtures, the validation of the resulting multi-component model is limited to n-heptane and n-decane mixtures.

All listed models fail in capturing switching between evaporation and condensation during the droplet lifetime, at least as they are proposed, which is mandatory to describe the vaporization of multi-component droplets composed of hydrophilic species. Hence, the present work proposes a novel numerical approach for single droplet evaporation. To attend this objective, a new formulation is rigorously derived from general transport equations for the gas phase. A specific attention will be devoted to the determination of the vapor-liquid equilibrium [13] and the diffusion coefficients, and we focus our work to binary liquid mixtures of various substances.

The remaining of this manuscript is divided in seven sections. Following this introduction, the modeling techniques are presented in a concise fashion whereas specific model derivations are placed in an appendix. Next, the solution strategy is presented, which is of fundamental importance to solve the resulting equations from the proposed modeling approach. Results are distributed in the following four sections, where different topics are systematically investigated. Finally, the paper is closed with some final remarks and an outlook in the ”Summary and conclusions” section.

2. Modeling description

In this section, our new modeling approach is described. Initially, the description on how the heat and mass transfers in the gas and liquid phase are handled is presented. The adaptation to convective effects is also included. Thereafter, the computation of the diffusion coefficients and the vapor-liquid equilibrium (VLE) is detailed.

2.1. Heat and mass transfer on a quiescent atmosphere: gas phase

The key aspects of the model derivation process are summarized in this section in terms of Eqs. 1-3 for the energy conservation, and 4-6 for the mass/species conservation. Both have been derived from the transport equations of energy and chemical species applied to the gas phase as detailed in the supplementary material, wherein modeling assumptions are gradually presented as soon as they are employed. Altogether, these can be summarized by:

1. Quasi-steady process;
2. Spherical symmetry;
3. Heat conduction is expressed in terms of the Fourier's law;
4. Mass diffusion is expressed in terms of the Fick's law;
5. Second order Soret and Dufour effects are neglected for heat and mass diffusion;
6. Source terms related to the species consumption (or production), as well as heat release due to chemical reactions, are neglected;
7. The low-Mach dilatable hypothesis is enforced;
8. Volumetric forces are not taken into account;
9. No net dissolution of inert gases onto the liquid phase;
10. Ideal gas formalism employed for the gas phase[1].

The energy conservation, here represented through the sensible enthalpy h, takes the following form after some manipulations:

$$\frac{d}{dr}\left(\rho u r^2 h\right) - \frac{d}{dr}\left(\lambda r^2 \frac{dT}{dr}\right) - \frac{d}{dr}\left(\sum_{k=1}^{N} \rho D_k h_k r^2 \frac{dY_k}{dr}\right) = 0, \tag{1}$$

[1]Even though the ideal gas simplification is assumed, non-ideal effects are considered in the liquid phase and the phase interface.

where ρ is the density, u is the velocity, r is the radial coordinate, λ is the thermal conductivity, T is the temperature, D_k is the diffusion coefficients from species k towards the multi-component gas mixture, and Y_k is the mass fraction. After integration, the following form is retrieved:

$$-4\pi\lambda r^2 \frac{dT}{dr} = \dot{m}_d \left[T(r) \sum_k c_{p,k}\varepsilon_k - T_s \sum_k c_{p,k}\varepsilon_k - \frac{\dot{q}_d}{\dot{m}_d} + L(T_s) \right], \tag{2}$$

where $c_{p,k}$ is the specific heat of species k at constant pressure, $\varepsilon_k = \dot{m}_k/\dot{m}$ the fractional evaporation rate of species k, $\dot{q}_d$ is the heat transfer rate entering the droplet and L is the mixture's latent heat. A second integration allows us to isolate the aforementioned heat transfer rate

$$\dot{q}_d = \dot{m}_d \left[L(T_s) - \frac{\sum_k c_{p,k}\varepsilon_k (T_\infty - T_s)}{B_T} \right]. \tag{3}$$

Subscripts $_s$ and $_\infty$ refer to quantities evaluated at the droplet surface and in the far field, respectively. Further, subscripts $_d$ and $_l$ are associated to droplet and liquid quantities. As for the species conservation equations in the gaseous phase, using the set of assumptions described before, one can depart from the following equation for each species k:

$$\frac{\dot{m}}{4\pi}\frac{dY_k}{dr} - \frac{d}{dr}\left(\rho D_k r^2 \frac{dY_k}{dr}\right) = 0, \tag{4}$$

which when integrated and combined with the definition of ε_k presented in [14] concerning the Fick's Law assumption, leads to the following expression:

$$\dot{m}\left[Y_k - \varepsilon_k\right] - 4\pi\rho D_k R^2 \frac{dY_k}{dR} = 0. \tag{5}$$

Note that considering all participating vapor species k, it follows that $\sum_k \varepsilon_k = 1$, or accordingly $\sum_k \dot{m}_k = \dot{m}$. Through integration, the global evaporation rate can be expressed as function of any species k:

$$\dot{m} = -\dot{m}_d = 4\pi R_d \rho D_k \ln\left|B_{M,k} + 1\right|, \tag{6}$$

where R_d is the instantaneous droplet radius. The terms B_T in Eq. 3 and $B_{M,k}$ in 6 refer to the Spalding energy and species k transfer numbers. Both are described by

$$B_T = \frac{(T_\infty - T_s)\sum_k c_{p,k}\varepsilon_k}{L(T_s) - \frac{\dot{q}_d}{\dot{m}_d}}, \quad \text{and} \quad B_{M,k} = \frac{Y_{k,s} - Y_{k,\infty}}{\varepsilon_k - Y_{k,s}}, \tag{7}$$

From the derived set of equations, it is important to notice that, in typical situations [2] when the diffusion coefficient D_k and the Spalding mass transfer number $B_{M,k}$ are determined, the complete net flux $\dot{m}_d$ from the droplet is obtained in terms of Eq. 6. Such an observation may lead to the interpretation that the computation of the contribution of only a single species is necessary. Nevertheless, this is not consistent, as information about all other participating species are implicitly included in ε_k, since the condition $\sum_k \varepsilon_k = 1$ must be attained.

If the simplification that all of the participating species present the same value for the diffusion coefficient is made, the determination of ε_k is straightforward. Under this condition, Eq. 6 would lead to $B_{M,k} = B_{M,m}$ for all k (see for instance [2]). However, when differential diffusion is accounted for, the determination of ε_k requires additional computational efforts.

The presence of the absolute operator in some expressions turn the solution of the derived equations set a challenging task. A consistent solution procedure is proposed in section 3.

2.2. Heat and mass transfer on a quiescent droplet: liquid phase

The equations presented in the previous section, which determine heat and mass transfer rates, have been derived considering only the gas phase. The resulting set of equations may lead to the interpretation that liquid phase information is not necessary, however such information is hidden in quantities evaluated on the droplet surface. Before addressing the employed approaches to describe the phase interface, the different treatments given to the liquid phase are indicated.

Two different approaches are described for the liquid phase: infinite liquid conductivity and diffusivity (ILCD), and full modeling of liquid transport phenomena. Following the assumptions of spherical symmetry, quiescent atmosphere, and no effects of gravity, both respectively deliver a zero-dimensional and an one-dimensional approach.

In agreement with the ILCD approach, the temperature within a droplet is uniform while it may vary along the time. An expression for it can be determined considering the heat transfer rate necessary to raise droplet temperature $\dot{q}_d$, as follows

$$mc_l \frac{dT_d}{dt} = \dot{q}_d \Rightarrow \frac{dT_d}{dt} = \frac{\dot{q}_d}{mc_l}, \tag{8}$$

[2] Exceptions occur, when the argument of the logarithm operator in Eq. 6 presents a singularity (e.g. $Y_{k,s} = Y_{k,\infty}$)

where t is time, m the droplet mass at t, and c_l the liquid specific heat.

With respect to the mixture composition in the liquid phase, the hypothesis of infinite liquid diffusivity leads to uniform values of species molar fractions within a droplet. As for the liquid temperature in the ILCD approach, the mixture composition may vary along the time. However, its determination is straightly achieved when solving the entire equation set, which includes the phase interface modeling.

When the heat and mass transfer processes in the droplet interior are accounted for, transport equations for energy and species mass fractions of the liquid phase are considered. Alternative models for describing the droplet's interior will be subject of subsequent works. It should be noted, however, that the coupling with the gaseous phase developments of Sec. 2.1 is straightforward, through the following boundary conditions at the droplet surface

$$\dot{q}_d = 4\pi R_d^2 \lambda_l \left.\frac{\partial T}{\partial r}\right|_{r=R_d}, \tag{9}$$

$$4\pi\rho_l D_k^L r^2 \left.\frac{dY_k^L}{dr}\right|_{r=R_d} = 4\pi\rho D_k r^2 \left.\frac{dY_k}{dr}\right|_{r=R_d}. \tag{10}$$

Equation 10 can be further combined with Eqs. 5 and 6 to obtain

$$\left.\frac{dY_k^L}{dr}\right|_{r=R_d} = \frac{\rho D_k}{\rho_l D_k^L} \frac{\ln\left|B_{M,k}+1\right|}{R_d} \left(Y_{k,s} - \varepsilon_k\right). \tag{11}$$

2.3. Convective heat and mass transfer

Some care must be taken when considering convective heat and mass transfer on a multi-component droplet while preserving the generality of the proposed approach. As a result from the derivations presented in the supplementary materials, convective heat and mass transfer can be considered in terms of

$$\dot{q}_d = 4\pi R\lambda \frac{Nu}{2}\left(T^\infty - T^s\right) - \dot{m}L \quad \text{and} \quad \dot{m} = 4\pi R\rho D_k \frac{Sh_k}{2} B_{M,k}. \tag{12}$$

Both equations are general, thereby both can be applied to describe evaporation and condensation processes. Limitations may arise according to the strategy adopted to compute the Nusselt Nu and the Sherwood Sh_k numbers.

In agreement with the classical model [13], a general approach is to consider that

$$Nu = \frac{\ln|B_T + 1|}{B_T} Nu^0 \quad \text{and} \quad Sh_k = \frac{\ln\left|B_{M,k} + 1\right|}{B_{M,k}} Sh_k^0, \tag{13}$$

where Nu^0 refers to empirical correlations derived from non-evaporating moving droplets, and Sh_k^0 is the analogous for mass transfer with Pr replaced by Sc (see Eq. 14). For instance, in the present work we employed the following expressions

$$Nu^0 = 2 + 0.57 Re^{1/2} Pr^{1/3} \quad \text{and} \quad Sh_k^0 = 2 + 0.57 Re^{1/2} {Sc_k}^{1/3}, \tag{14}$$

where $Re = \rho|u_\infty - u_d|d_p/\mu$ is the Reynolds number, u_∞ the velocity of the bulk flow, u_d the droplet's velocity, d_p the droplet diameter, μ the dynamic viscosity, Pr the Prandtl number, and $Sc_k = \mu/\rho D_k$ the species k Schmidt number.

Specific limitations emerge when empirical correlations derived for evaporating droplets replace Nu and Sc_k in Eq. 12, or when models based on the film theory (e.g. [9]) are envisaged. When using these strategies, attention must be paid on the fact that equations have been derived for limited values of the Spalding numbers. For example, in Abramzon and Sirignano [9] model the Falkner-Skan solutions (see [2]) used to obtain the correction factor F were derived for a range of $0 \leq B \leq 20$ [13], where B refers either to B_T or B_M. Specifically to the Abramzon and Sirignano [9] model, a strategy to attenuate such limitations is to consider a Spalding number based on the gaseous mixture for the computation of F as proposed by Tonini and Cossali [6]

$$B_M = \frac{\sum_{\text{vapor}} Y_k^s - \sum_{\text{vapor}} Y_k^\infty}{1 - \sum_{\text{vapor}} Y_k^s}, \tag{15}$$

where the subscript $_{\text{vapor}}$ implies the summation is ignoring all inert species. Accordingly, the limitations presented by possible negative values of $B_{M,k}$ are attenuated by the summation operator. Nevertheless, this approach implies that differential diffusion effects are neglected[3] within the film, while this diffusive transport is considered in the modified Nusselt and Sherwood numbers as follows

$$Nu^* = 2 + \frac{Nu^0 - 2}{F_T} \quad \text{and} \quad Sh_k^* = 2 + \frac{Sh_k^0 - 2}{F_M}, \tag{16}$$

[3]The Spalding number of the gas mixture is obtained when the assumption that all participating species have the same value for the diffusion coefficient (i.e. $D_k = D$) is made.

in which F_T and F_M are the correction factors respectively for thermal and species k film thicknesses due to Stefan flow effects, given by

$$F = (1 + B)^{0.7} \frac{\ln(B + 1)}{B}, \tag{17}$$

where B refers to B_T and B_M correspondingly.

2.4. Modeling of diffusion coefficients

As the evaporation rates are proportional to mass diffusion coefficients, a distinct attention must be devoted to their evaluation, specifically on two aspects: the determination of binary diffusion coefficients, and the approaches used to estimate the diffusion coefficient of a species into a mixture. The last approach is typically connected to the first one, as it is often formulated in terms of binary diffusion coefficients. Nevertheless, both approaches are independent and, for each one, different modeling strategies can be applied.

With respect to the approaches used to estimate binary diffusion coefficients, special attention is given to the so-called Fuller method (FM) [15–17] due to its use in previous works (e.g. [3, 18]) and its additive formulation which aligns with the UNIFAC approach (see section 2.5). According to this method, binary diffusion coefficients can be estimated by

$$D_{ij} = 0.00143 \frac{T^{1.75} \left(\frac{1}{M_i} + \frac{1}{M_j}\right)^{1/2}}{P \sqrt{2} \left(\sum_i v_k^{1/3} + \sum_j v_k^{1/3}\right)^2}, \tag{18}$$

where M_i is the molar mass of species i, P the ambient pressure, and $\sum_i v_k$ the summation of atomic diffusion volumes that composes species i. The determination of the diffusion volumes is based on the application of a non-linear least squares optimization analysis over experimental databases of binary diffusion coefficients of various substances [15, 16]. In [15, 16], Fuller and co authors defined specific values of diffusion volumes for some molecules, which do not always coincide with the corresponding summation procedure of atomic diffusion volumes. In a first moment, this called our attention on how to represent the binary diffusion coefficient of ethanol with other substances, since our first investigations were conducted with ethanol/water mixtures and deviations were noticed between computations and experimental data. As noticed in Fig. 2 (a), comparisons between experimental data and D_{ij} values obtained in the two cases labeled by

Air 1966 and *Air 1969* (both referring to computations performed with atomic diffusion volumes extracted respectively from [15] and [16]) show a better agreement with the lowest range of values achieved experimentally. Such a model performance is also noticed for water diffusion in air, as presented in Fig. 2 (b). Specific diffusion volumes are presented for water in [15, 16], which do not coincide with the corresponding summation of hydrogen and oxygen atomic volumes. The good agreement observed for water-air mixtures corroborates the observation made in [15] that the consideration of specific diffusion volumes for some substances improved model accuracy. Particularly, the experimental database employed in that work considered four data points for water-air mixtures while only one for ethanol-air (D_{ij} = 0.135 cm^2/s at T=298.2 K), which may point out that the consideration of additional experimental data could improve the prediction ability of the method for ethanol-air mixtures.

Rigorously, the diffusion of a substance in air is not a strict binary diffusion process, since air is a mixture of predominantly two substances, i.e. oxygen O_2 and nitrogen N_2. The constant composition of air in most engineering applications may be a justification to treat it as a pure substance, as done in [15] and [16]. Accordingly, diffusion volumes for air can be found. Thus, we investigate the behavior of the Fuller method when the diffusion of a substance in air is accounted for as a multi-component diffusion problem, as it is. Hence, in both Fig. 2, results achieved following a multi-component diffusion modeling with diffusion volumes obtained in [15] and [16] are respectively presented under *MC 1966* and *MC 1969* labels. For such computations, it is assumed that the concentration of the vapor species does not interfere with the value of the multi-component and the binary diffusion coefficients as given by Eq. 20. The diffusion coefficients computed with the multi-component approach demonstrate a similar behavior when compared with the simplification of air as a single species in Fig. 2. As for ethanol or water, the multi-component approach gives higher values of diffusion coefficients in both scenarios, showing a better agreement with the experimental data. Hence, the Fuller method shows a better performance for the computation of diffusion coefficients of vapor in air when air is represented by a multi-component mixture.

As mentioned in [19], there is no consensus in the literature concerning the computation of multi-component diffusion coefficients D_k when the Fick's Law is applied. Rigorously, the usage

of multi-component diffusion coefficients D_k with the Fick's Law requires an additional artifice to preserve both identities $\sum_{k=1}^{N} Y_k V_k = 0$ and $\sum_{k=1}^{N} Y_k = 1$ (V_k is the diffusion velocity - more details in the supplementary material). As pointed out in [14, 19], this artifice can be the consideration of a correction velocity or the specification of D_k for $N - 1$ species which are present in trace amounts. In our implementations, D_k is only computed for vapor species and no correction velocity is included. This approach does not differ from the applied strategies for instance in [6, 8] and resembles the second listed artifice to attain the two identities. Nevertheless, the impact of such an approach requires further studies which may be subject of future work.

Due to the previously mentioned lack of consensus concerning the computation of D_k, two approaches have been analyzed in the present work. The first corresponds to so-called Blanc's law [20, 21] which is commonly used in simulations of multi-component droplet evaporation [6, 18]. Following the formulation presented in [21, 22], D_k is given by

$$D_k = \left(\sum_{j \neq k}^{N} \frac{X_j}{D'_{kj}} \right)^{-1}, \tag{19}$$

in which D'_{kj} refers to the binary diffusion coefficient of species k and j evaluated in the actual multi-component mixture. As mentioned in [22], D'_{kj} is not quite the same as the corresponding binary diffusion coefficient D_{kj}, where the difference between both corresponds to the weak dependence of D'_{kj} on the whole multi-component mixture composition. However, as already highlighted by Marrero and Mason [22], deviations between both coefficients are at most of few percent and the assumption $D'_{kj} \approx D_{kj}$ is a reasonable approach. Therefore, we assume that $D'_{kj} = D_{kj}$ in the present study. It is important to mention that, some works present Eq. 19 in terms of mass fractions [6, 18], where X_j is switched by Y_j while $D'_{kj} = D_{kj}$.[4]

The second tested approach is given by

$$D_k = (1 - X_k) \left(\sum_{j \neq k}^{N} \frac{X_j}{D_{kj}} \right)^{-1}, \tag{20}$$

which is evaluated in [23] within the context of flame speed computations and pointed out in [14]

[4] In all the computations performed here with models obtained from [6], calculations of D_k follows Eq. 19 expressed in terms of mass fractions.

as a quantitatively correct approach. By comparing Eq. 20 with the Blanc's law, it is not difficult to identify that the term $(1 - X_k)$ in Eq. 20 turns D_k independent on the concentration of species k. Although the studies presented by Sandler and Mason [21], and Marrero and Mason [22] as well, indicated from derivations within the Chapman-Enskog kinetic theory that there is a dependence of the concentration of species k on D_k, experimental investigations presented in [24] demonstrated that such a dependence is not general. Studies conducted with diffusion of methanol and chloroform vapors at different molar fractions in air indicated that the multi-component diffusion coefficient varies for chloroform but it is predominantly constant for methanol. Mrazek et al. [24] point out that the observed differences of substance behavior are assigned to the differences of substances mass fractions, which agrees with the rationale presented in the investigations performed for binary diffusion coefficients in [25] and [26]. Hence, for mixtures where participating species present similar molar masses, Eq. 20 may be a suitable approach.

To choose the right formulation to estimate the multi-component diffusion coefficient, we considered the following rationale. In [21], deviations from the Blanc's law were investigated by means of the Chapman-Enskog kinetic theory. There, the Chapman-Enskog method is algebraically manipulated to resemble Blanc's law. By comparing the resulting equation with that of Blanc's law, an expression for the deviation could be obtained. Sandler and Mason [21] presented solutions of the derived deviation equations only for the special case of diffusion of a trace species through a quiescent mixture, specifically when $X_k = 0.0$. Although within this context the Blanc's law was demonstrated to be exact for certain cases, effects of variations in species k mass fraction on deviations of the Blanc's law were not quantified. In view of this aspect, the low variation of diffusion coefficients with vapor molar fractions in experiments conducted in [24], and the high complexity associated with implementations of more accurate models, we preferentially use Eq. 20 in our implementations. Still, it should be noted that any alternative formulation for computing the diffusion coefficients of a species toward a mixture could be applied to the current modeling strategy with no further difficulties. As such, a more detailed analysis of such approaches in multi-component droplet evaporation will be subject of future works.

2.5. Phase Interface: vapor liquid equilibrium

The description of the composition at the interface is of key importance to the entire modeling strategy. In the present study, it is assumed that the thermodynamic equilibrium is maintained in all tested scenarios. Nevertheless, two approaches have been adopted to represent the so-called vapor-liquid-equilibrium (VLE).

Within the thermodynamic equilibrium hypothesis, the fugacity of a liquid species k equals the fugacity of its vapor. By considering the representation of the fugacity in terms of activity coefficients, the VLE hypothesis allows the expression of the molar fraction of liquid species k (X_k^L) in terms of the molar fraction of its vapor (X_k^V) as follows

$$X_k^V P = X_k^L \gamma_k P_{\mathrm{vp},k} \mathcal{F}_k, \tag{21}$$

where γ_k is the activity coefficient of species k, P_{vp} the vapor pressure, and $\mathcal{F}$ a correction factor to include effects of real substances. Poling et al. [27] references that for subcritical components, $\mathcal{F}_k$ is often 1. Since our analysis are conducted at atmospheric pressure, this simplification is applied. Further simplifications can be done when γ_k is assumed as 1, which characterizes the Raoult's law.

The two approaches applied to address the VLE refer to the Raoult's law and the general UNIFAC activity coefficient model as described in [27]. This strategy, also adopted for instance in [18], allows to analyze ideal and non-ideal effects in the VLE description of different mixtures.

To evaluate the performance of the implemented VLE approaches, Fig. 3 shows the boiling-point diagram of three selected mixtures at atmospheric pressure, which are further analyzed in section 4. The selected mixtures refer to typical fuel mixtures, namely n-hexadecane/n-heptane, ethanol/iso-octane, and ethanol/water (hydrous ethanol). This specific choice was also made in order to be comprehensive in terms of the generality of mixture polarities - herein, we analyze all possible combinations: non-polar + non-polar (NN), polar + non-polar (PN), and finally polar + polar (PP).

The results presented in Fig. 3 gradually evolve in terms of the complexity associated with the interactions between components. The vapor-liquid equilibrium for the alkane mixture (Fig. 3(a)) is relatively simple, even though n-heptane is considerably more volatile than n-hexadecane.

Differences between Raoult's law and the UNIFAC method are minor, which is expected for most combinations of n-alkanes under atmospheric pressure [28].

In contrast to the alkane mixture, both the ethanol/iso-octane and the ethanol/water mixtures feature strong non-ideal behaviors - this is illustrated by the difference between the ideal formulation (Raoult's law) and a non-ideal formulation (here applied through the UNIFAC method). Both also exhibit an azeotrope point, wherein the composition of the vapor phase is indistinguishable from the composition of the gaseous phase.

When comparing the results presented in Fig. 3(b) and Fig. 3(c) with the experimental data, a good agreement can be noticed. Such an aspect successfully validates the implemented UNIFAC procedure to describe the VLE.

3. Solution strategy

Regarding the proposed modeling, two aspects require a special attention to address droplet heat and mass transfer in general ambient compositions. One concerns the absolute operator, while the other refers to the consideration of the fractional evaporation rate of species k (ε_k).

The discontinuous behavior of the absolute operator requires that the solution proceeds in different ways, according to the arguments of such an operator. However, the choice for a specific way requires some arbitrariness in the solver implementation, as floating point operations are considered. This aspect was the main motivation for the usage of a coupled procedure to solve the derived equations. Within this procedure, Eqs. 22-24 and the continuity equation build up a system of non-linear equations which is solved at once instead of solving each equation individually (i.e. uncoupled solver). As a result, the mentioned arbitrariness are resumed to those intrinsic to the chosen non-linear system solver.

While the discontinuities imposed by the absolute operator could be managed by the choice of a coupled procedure for the solver, the consideration of ε_k in the equation set presented in section 2 imposes another challenge for the solution algorithm: division by zero when $\dot{m} = 0$. Such a condition has a different interpretation in the context of multi-component liquids than in single component cases. In this case, when having $\dot{m} = \sum_k \dot{m}_k = 0$, it does not necessarily mean that all $\dot{m}_k$ are zero, but rather, that they can have different contributions of evaporation/condensation.

To overcome this issue, the so-called m-based approach has been derived, in which the ε_k are expressed in terms of their definition $\dot{m}_k/\dot{m}$ in all equations of Sec. 2. Such a strategy is of fundamental importance for a robust method capable to describe phase change in general atmosphere compositions. In analogy with the m-based approach, the strategy of expressing the equations set in terms of ε_k are referred as the ε-based approach. More details about the derivations of both approaches are found in the supplementary material of this manuscript.

As the m-based approach is more robust than the ε-based one (see section 5), the m-based is adopted as the main solution strategy in the present manuscript. Except when explicitly mentioned, this strategy is the one employed in our investigations. The remaining of this section focus in the m-based approach as well, since the achievement of the corresponding equations for the ε-based approach is straightforward.

Within the m-based approach, the following set of equations is considered.

$$\dot{m}_k = \frac{\dot{m}\left(Y_k^s - \delta_{\dot{m}_k}^{\text{abs}} Y_k^\infty \zeta_{\dot{m}_k}\right)}{1 - \delta_{\dot{m}_k}^{\text{abs}} \zeta_{\dot{m}_k}}; \;\; \text{if} \;\; \frac{\dot{m}_k - \dot{m} Y_k^\infty}{\dot{m}_k - \dot{m} Y_k^s} > 0 \;\; \delta_{\dot{m}_k}^{\text{abs}} = 1, \;\; \text{else} \;\; \delta_{\dot{m}_k}^{\text{abs}} = -1 \tag{22}$$

$$\dot{q}_d = \frac{\sum_k \dot{m}_k c_{p,k}(T^\infty - T^s)}{\zeta_{\dot{q}_d} - \delta_{\dot{q}}^{\text{abs}}} - \sum_k \dot{m}_k L_k; \;\; \text{if} \;\; (1 + B_T) > 0 \;\; \delta_{\dot{q}}^{\text{abs}} = 1, \;\; \text{else} \;\; \delta_{\dot{q}}^{\text{abs}} = -1, \tag{23}$$

where

$$\zeta_{\dot{m}_k} = \exp\left[\frac{\dot{m}}{4\pi R_d \rho D_{k,m}}\right], \quad \zeta_{\dot{q}_d} = \exp\left[\frac{\sum_k \dot{m}_k c_{p,k}}{4\pi R_d \lambda}\right], \tag{24}$$

with B_T expressed in terms of $\dot{m}_k$ on Eq. 7. Finally, the global mass conservation closes the equation set, namely $\dot{m} = \sum_k \dot{m}_k$.

Regarding the absolute operator in the equations of heat and components mass transfer rates, two expressions for each one of these transfer rates are implemented as seen in Eqs. 22-23. At each time step, a check is made to determine which expression will be chosen by the solver in agreement with the argument value of the absolute operator. Here, this procedure is encapsulated through the δ unitary variables.

Following this equation set, the problem is therefore well defined, by having $k+2$ equations for $k+2$ variables to be determined ($\dot{m}_k$, $\dot{m}$, and $\dot{q}_d$). The system of non-linear equations is then solved at each time step in a dedicated numerical code written in Python. To accomplish the solution

of the non-linear system the Scipy library is considered, more specifically the Optimize module through the function fsolve [29]. This function is a wrapper around MINPACK's hybrd function [30] which itself is a modification of the Powell method [31]. This function operates trying to find zeroes to residual expressions, i.e. the solver is fed with guesses (superscript ^{G} below) expected to be close to the actual converged values which lead to residuals $\mathcal{R}$ obtained at each time step:

$$\dot{m}_k^G - \frac{\dot{m}^G\left(Y_k^s - \delta^{\text{abs}}_{\dot{m}_k^G} Y_k^\infty \zeta_{\dot{m}_k^G}\right)}{1 - \delta^{\text{abs}}_{\dot{m}_k^G}\zeta_{\dot{m}_k^G}} = \mathcal{R}_{\dot{m}_k};\ \text{ if } \frac{\dot{m}_k^G - \dot{m}^G Y_k^\infty}{\dot{m}_k^G - \dot{m}^G Y_k^s} > 0\ \ \delta^{\text{abs}}_{\dot{m}_k^G} = 1,\ \text{ else } \delta^{\text{abs}}_{\dot{m}_k^G} = -1, \tag{25}$$

$$\dot{q}_d^G - \frac{\sum_k \dot{m}_k^G c_{p,k}(T^\infty - T^s)}{\zeta_{\dot{q}_d^G} - \delta^{\text{abs}}_{\dot{q}^G}} + \sum_k \dot{m}_k^G L_k = \mathcal{R}_{\dot{q}_d};\ \text{ if } (1 + B_T^G) > 0\ \ \delta^{\text{abs}}_{\dot{q}^G} = 1,\ \text{ else } \delta^{\text{abs}}_{\dot{q}^G} = -1, \tag{26}$$

3.1. Initialization

Here we decribe the initial guesses. The global evaporation rate is computed by

$$\dot{m}^{\text{init}} = 4\pi R_d \rho \bar{D} \ln(1 + B_M), \tag{27}$$

where the superscript $^{\text{init}}$ stands for a guess used only at the initialization. Note that, at the initialization, the result of a preferential diffusion problem is assumed to define the global evaporation rate and the averaged Spalding mass transfer number is employed, i.e. Eq. 15. The average diffusion coefficient $\bar{D}$ on Eq. 27 is computed in the same manner as in [6], namely

$$\bar{D} = \frac{\sum_{\text{vapor}} Y_k^{ref} D_k}{\sum_{\text{vapor}} Y_k^{ref}}, \tag{28}$$

in which Y_k^{ref} is the reference mass fraction inside the film region for each species k. Notice however that the summations are carried ignoring all inert species. In this work, the computation of Y_k^{ref} follows the one-third rule between mass fractions on infinity and at the surface of the droplet, namely, $Y_k^{ref} = 1/3 Y_k^\infty + 2/3 Y_k^s$. Once the first global evaporation rate (Eq. 27) is computed, the evaporation rates of each individual species are abstracted from the definition of $B_{M,k}$, such that

$$\dot{m}_k^{\text{init}} = \dot{m}^{\text{init}}\left(Y_k^s + \frac{Y_k^s - Y_k^\infty}{B_M}\right) \tag{29}$$

Then, the assumption that $B_T = B_M$ is made for the purposes of initializing the heat entering the droplet (since B_T depends on $\dot{q}_d$ which itself needs to be initialized):

$$\dot{q}_d^{\text{init}} = \frac{\sum_k \dot{m}_k^{\text{init}} c_{p,k}(T^\infty - T^s)}{\zeta_{\dot{q}_d}^{\text{init}} - \delta_{\dot{q}}^{\text{abs,init}}} - \sum_k \dot{m}_k^{\text{init}} L_k;\ \text{ if } (1 + B_M) > 0\ \ \delta_{\dot{q}}^{\text{abs,init}} = 1,\ \text{ else } \delta_{\dot{q}}^{\text{abs,init}} = -1, \tag{30}$$

Following this procedure, a first guess to $\dot{m}$, $\dot{m}_k$, and $\dot{q}_d$ is computed. These values are then fed into the non-linear solver through Eqs. 25-26 which allow the simulation to start.

3.2. Further details

The time integration is performed using RK-23 or RK-45 Runge Kutta schemes throughout our analyses, both implemented inside the Scipy python module [29]. The results achieved from the initialization process are then used as guesses to start the first iteration. For next iterations, the necessary guesses for the current iteration are chosen to be the converged results of the previous iteration. The convergence of the solver is controlled through an absolute tolerance for each variable as well as a relative tolerance applied to all variables.

The "one-third rule" as seen in [9] is applied when computing all the average thermodynamic and transport properties inside the film region, since these properties are regarded as constant in space to allow for the integration. This is done through reference mass/molar fractions (as shown in Sec. 3.1) as well as a reference temperature.

To account for convective heat and mass transfer, Equation 12, when converted to the above solution strategy, follows the same structure, namely, the set of equations 22-23 but switching the ζ factors presented in both expressions in Eq. 24, respectively by T2308

4. Influence of the VLE approach

As previously mentioned, the Vapor-Liquid Equilibrium is a key aspect for the modeling of multi-component droplet heat and mass transfer. Therefore, it is the purpose of this section to evaluate the performance of the proposed modeling strategy combined with different VLE approaches.

In order to encompass a good representation of typical fuel mixtures, the vapor-liquid equilibrium approaches are analyzed for three binary mixtures of fuels: n-hexadecane/n-heptane, ethanol/iso-octane, and ethanol/water (hydrous ethanol). As discussed in section 2.5, these binary mixtures allow for the exploration of a general set of mixture polarities - namely: NN, PN, and PP. Simulations are conducted for droplets with initial diameters $d_0 = 50\mu m$, for varying initial volume fraction VF and initial temperatures. The surrounding gas temperature is always set to be

the same as the initial temperature of the droplet, namely $T_\infty = T_{d,0}$. For both the ethanol/water as well as the ethanol/iso-octane droplets, initial temperatures are set at $T_{d,0} = 304K$. For the n-hexadecane/n-heptane droplets, different initial temperatures are used for each composition, as these are extracted from the experimental investigations conducted by Wilms [28]. Results follow on Figs. 4-5 for the normalized surface area (d^2/d_0^2) as well as its temperature.

As expected from the boiling-point diagrams from Fig. 3, there is no significant difference between Raoult's law and the UNIFAC method for n-hexadecane and n-heptane mixtures, and there is a good agreement with the experimental data. The strong variation in diameter decay for the different initial conditions is well captured by the model. Such a performance demonstrates the good coupling between heat and species mass transfer rates achieved with the proposed model.

Despite not shown here, a good agreement with the experimental data presented in [28] could be observed for n-tetradecane and n-hexadecane mixtures, as achieved in [18] where the model proposed in [6] was applied. We decided, however, to show results of a n-hexadecane and n-heptane mixture as the volatility of the two components are quite different between each other. Such a characteristic allows a better evaluation of the robustness of the proposed model. Particularly, to all the simulated cases here, high volatile species have been considered.

No differences between Raoult's law and the UNIFAC method are visible at the single-component extremes for the ethanol/iso-octane (Fig. 5 top) and the ethanol/water (Fig. 5 bottom) cases, as both VLE methods shall behave the same in single component cases. However, for intermediary compositions, great differences can be spotted on the behavior of the evaporative process, even though the predicted droplet lifetime is nearly the same. For the ethanol/iso-octane case, there is also considerable difference in the predicted temperature at the end of the droplet lifetime. Differences in the prediction of droplet temperatures for ethanol/water mixtures do also occur, but not so well pronounced as for ethanol/iso-octane mixtures. Such an outcome indicates the strong coupling among heat and species mass transfer rates with the VLE approaches.

The results presented in this section reinforce the main outcomes obtained in the previous study [18], where simulations were conducted with the [6] model and the same UNIFAC algorithm as used here. Indeed, the Raoult's law is insufficient to describe the VLE of non-ideal liquid mixtures, which is reflected in the prediction of typical droplet evaporation-related metrics. Nevertheless, in

the results presented in this section, both tested VLE approaches deliver similar droplet lifetime, which may be an important indicative for investigations on real sprays. For instance, comparisons between spray penetration lengths may be insufficient to evaluate if a multi-component spray is well predicted by a CFD model based on the ideal VLE approach. Perhaps, droplet size distribution acquired throughout the spray flow may prove to be useful to address such an issue.

5. Droplet heat and mass transfer in atmospheres with high vapor concentration

As mentioned in the introduction of this manuscript, the consideration of combustion processes of hydrophilic fuels in spray flows imposes a quite challenging scenario: droplet heat and mass transfer in atmospheres with high mass fractions of a liquid vapor species. Indeed, this is not specific to the combustion of liquid hydrophilic fuels, but may also occur in any flow where liquid droplets interact with atmospheres composed of varying vapor mass fractions crossing the saturation values defined by the droplet surface temperature and the ambient pressure. In a more pragmatic viewpoint, such operating conditions impose a stress point wherein the current model proposition is found to bypass it where other formulations fail. The investigation of such operating conditions follows the study conducted by Law et al. [32] in this section, where droplets of liquid methanol (hydrophilic fuel) interact with air atmospheres at different relative humidity values. Afterwards, models are tested in more severe conditions which mimic the interaction of hydrophilic fuel droplets with freely propagating laminar flames.

Single droplet evaporation cases in quiescent atmospheres are conducted with pure methanol, in which the initial diameter is set to $d_0 = 1.6mm$ and both liquid and air temperatures are $T_{d,0} = T_\infty = 298K$. A first case is defined for zero relative humidity ($\phi = 0$) and then a second one for the maximum relative humidity ($\phi = 1.0$) at this temperature. For each simulation, three different implementations are compared with results extracted from [32], namely, both the m-based and the ε-based approaches of the proposed model, and finally the formulation present in [6] as well. Particularly, the model proposed by Tonini and Cossali [6] is used as a reference in the present work as previously done in [18]. Results are displayed in Fig. 6.

As seen in Fig. 6 (top), there is no difference between all three formulations for the case with no air humidity - this is somewhat expected since the droplet stays single-component throughout its

lifetime, with initial conditions that ensure only evaporation occurs (no condensation). However, for the case with maximum relative humidity, the formulation as presented by Tonini and Cossali [6] detaches itself from the two other formulations, predicting a lower temperature which translates into a slower evaporation rate.

It has to be mentioned that none of the simulations conducted here includes the heat transfer process through the support fiber that holds droplets in the experimental apparatus. The inclusion of such an effect is supposed to increase the evaporation rates and to reduce the deviations noticed among simulation results and experimental data [33].

In agreement with the previous tests, a pure methanol droplet is used to stress the chosen modeling strategies in more severe conditions. Hence, a droplet of initial diameter $d_0 = 20\mu m$ is injected with initial temperature $T_{d,0} = 300K$ into an atmosphere of the same temperature, $T_\infty = 300K$. However, this droplet was injected with velocity $U_{d,0} = 0.5m/s$ into an atmosphere with velocity $U_\infty = 0.5m/s$ such that no drag effects are present even though the droplet is moving. This droplet moves through a first zone of length $L_0 = 0.5cm$ to then meet the representation of a flame-front, here described through a hyperbolic tangent profile rising from a temperature of $T_\infty = 300K$ to approximately $T_\infty = 2000K$ and a water composition at infinity rising from $Y_{\infty,Wat} = 0$ to approximately $Y_{\infty,Wat} = 0.15$. These atmospheric conditions aim to represent a freely propagating one-dimensional flame of general hydrocarbons where the mass fraction profile of water reaches the maximum value of a stoichiometric combustion reaction of methanol in air. The region defined by the hyperbolic tangent profile is set to be $L_{flame} = 0.1mm$, in view of the representation of a general hydrocarbon flame thickness. Results follow on Fig. 7.

The results presented in Fig. 7 clearly demonstrate the robustness of the m-based approach of the proposed model, as this is the only approach able to carry the simulation until the end of the droplet lifetime. Moreover, all three formulations perform in practically identical fashion up until other formulations stop working. The first formulation to fail is the one of Tonini and Cossali [6], because the droplet enters in a regime for which the absolute value is needed in order for the simulation to proceed. After some time inside this regime, the ε-based approach fails. Such a limitation occurs because of the fact that droplet temporarily starts to condensate - therefore, passing the critical point of $\dot{m} = 0$ wherein any fractional evaporation rate ϵ is mathematically

undefined. Therefore, it is possible to see that the m-based approach is able to handle cases in which a droplet evaporates, then condensates and then evaporates again, with parameters varying in a steep manner as can be found in combustion process of hydrophilic fuels.

6. Importance of differential diffusion modeling

As long as differential diffusion effects are accounted for, the evaporation preference of participating liquid species does not follow the predicted behavior by simplified approaches. Hereafter, we refer to such a behavior as the inversion problem. The inversion of the evaporation preference of vapor species in multi-component droplets have been noticed for instance in [34], which is comprehensively explored in terms of the so-called separation factor. In that work, it could be noticed that the inversion problem was triggered by the consideration of ideal and non-ideal VLE approaches. Nevertheless, in [34] such an investigation was limited to the VLE modeling as no differential diffusion was accounted for. Following the present analysis, which does not intend to be exhaustive in the topic, the inversion problem is limited to mixtures where nonpolar substances and non-ideal VLE approaches are considered. It should be noted however that this behavior seems to be universal to differential diffusion formulations, since the inversion phenomena can also be observed when employing the procedure proposed by [6] as well, as shown in this section.

Figure 8 (top) illustrates the inversion problem in terms of the normalized droplet surface area and internal mixture composition for a ethanol/water binary mixture. Simulations are conducted for droplets of initial diameter $d_0 = 20\mu m$, the same initial temperature as the gas in the far field $T_{d,0} = T_\infty = 300K$, and an initial composition of $VF_{\text{ethanol}} = 0.95$. For all simulations, the non-ideal VLE was characterized through the UNIFAC formulation. The relative air humidity is set to $\phi = 0$.

Two models constructed in a differential diffusion (DD) framework (the model proposed here and the one proposed in [6]) are compared with a simplified formulation of the m-based approach within a preferential diffusion (PD) framework. To achieve the preferential diffusion scenario, instead of using a diffusion coefficient for each individual species, a global, average diffusion coefficient is applied (i.e. Eq. 28). To compute this global coefficient, the diffusion coefficients D_k are computed with the same formulation as in [6]. Also noteworthy is that, the index k in

Eq. 28 only scans through the vapor species, with inert species not taken into account, such that $\sum_{k=1}^{N} Y_k^{ref} < 1.0$ for instance. Therefore, the diffusion coefficient computed for the preferential diffusion approach through Eq. 28 represents a case in which all liquid species can be clumped together as a single vapor diffusing in binary fashion towards a single, clumped inert species.

The three compared approaches depict quite similar results for the evolution of the normalized droplet surface area. However, differences on the droplet internal composition are quite clear with the treatment given to the diffusive transport of species. In both models based on the DD approach, water leaves the droplet at first, delivering a pure ethanol droplet at the end of the evaporation process. On the other hand, when the PD approach is accounted for, ethanol leaves the droplet at first despite composing 95% of the initial volume fraction of the liquid.

The behavior observed with the PD approach sounds intuitive due to the highest volatility of ethanol when compared with water. Nevertheless, bearing in mind that the diffusive transport is decisive to define the mass transfer in a evaporating droplet (as such a phenomenon define the so-called hydrodynamic evaporation models [13]), another aspect competes with the component volatility: the diffusion coefficient D_k. Water molecules are lighter than ethanol ones. As a result, diffusion coefficients of water are larger than those of ethanol as seen in Fig. 2. Such a characteristic implies that water molecules can travel faster than ethanol molecules in air, allowing a higher flux of water away from the droplet surface.

During the development of our investigations, we also observe that different modeling strategies for the computation of the non-ideal VLE, the binary and multi-component diffusion coefficients affect the condition in which the inversion problem is triggered. Nevertheless, such an influence is small, and any combination of such models does not manage to inhibit this effect. Considering these aspects, some investigations are conducted in order to evaluate the influence of specific variables on the triggering of the inversion problem. Specifically, the vapor concentration in the far field demonstrated to be a key parameter in this issue. Hence, the influence of the air humidity is investigated in what follows.

Simulations follow the same ambient conditions applied to the case presented in Fig. 8(top), i.e. ethanol/water droplets with $d_0 = 20\mu m$, $T_{d,0} = T_\infty = 300K$, and $VF_{\text{ethanol}} = 0.95$. The relative air humidity is increased and Fig. 8(bottom) showcases the results for $\phi = 0.4$, through

the normalized droplet surface area and the internal composition of the droplet.

As seen in Fig. 8, as the relative humidity is increased, differences in the prediction of the droplet lifetime start to become more apparent between the different models. Also, the behavior in predicting the internal composition evolution can be quite different. Along with the development of this study, various tests have been conducted varying the relative humidity. From these investigations it could be noticed that the inversion problem ceases as long as the relative humidity is higher than approximately $\phi \approx 0.025$. From this value, the behavior shifts towards those presented in Fig. 8 (bottom), that is, ethanol evaporates first, leaving a single-component water droplet characterized by a slower evaporation rate and the change in the slope of the normalized surface curve.

From the results presented in Fig. 8 it is clearly noticed that the choice of the diffusion transport approach does interfere with the heat and mass transfer processes in a droplet. According to such an approach and the surrounding gas compositions, the sequence that the vapor of a specific component is released from the droplet surface is defined. Such an outcome requires a special care to CFD simulations of multi-component sprays, where dry air is typically employed as the carrier gas. In particular to combustion applications, the order in which a species is released from the droplet may affect the mixture preparation process and, consequently, the evolution of chemical reactions. Nevertheless, as soon as more realistic air compositions are considered, which accounts for air humidity, problems should be attenuated when multi-component droplet models based on differential-diffusion are applied.

6.1. Influences of multi-component diffusion coefficient approaches

The different possibilities to address the multi-component diffusion coefficient D_k claim for an investigation about the influence of these possibilities on the computation of heat and mass transfer of multi-component droplets. In view of this, the different approaches presented in section 2.4 to estimate the multi-component diffusion coefficient are tested in this section. Herein, only the proposed model following the *m*-based approach is considered.

Altogether two approaches are analyzed, the Blanc's law as given by Eq. 19 and the one proposed by Coffee and Heimerl [23]. Initially, simulations ran for the exact same ethanol/water test

cases presented in Fig. 8; however, no notable differences were spotted between both approaches. Deviations between both approaches become noticeable when the temperature of the surrounding gas and the vapor mass fraction of water was increased, resembling conditions more representative of droplets interacting with flames.

Figure 9 presents the evolution of the liquid components mass fractions and the temperature of droplets in quiescent atmospheres at $T_\infty = 1500K$ and with water vapor mass fractions of 0.0 and 0.1, respectively. In both figures, deviations between both tested approaches can be noticed.

As seen on Fig. 9, for a high-temperature environment, both formulations can not only showcase differences in the transitory behavior of the droplet evaporation, but also notably on the maximum temperature of the droplet. This behavior can be justified by the different values of the multi-component diffusion coefficients delivered by each approach, which are directly connected with the main driven mechanism for the mass transfer process. Certainly, changes on the liquid temperature are associated with the clear coupling between heat and mass transfer processes, which is strongly valued throughout the derivation and solution process of the proposed approach.

In fact, the noticed modification on liquid composition and temperature indicates that the choice for a specific model to represent the multi-component diffusion coefficient affect the exchange rates of heat and components masses between both phases. Consequently, this may interfere with CFD predictions of multi-component spray flows in high temperature atmospheres. However, it is necessary to highlight that, in contrast to the consideration of differential diffusion effects, such differences are limited to a specific range of gas temperature and vapor mass fractions. Subsequent works are planned to investigate the influence of different approaches of the multi-component diffusion coefficients for the prediction of multi-component heat and mass transfer in more details.

7. Model performance in convective heat and mass transfer

Special attention is paid to the influence of taking or not into account the correction factor for Stefan flow effects for convective heat and mass transfer, showcased in Eqs. 16 and 17. This comparison was motivated by the limitations of correction factors based on the film-theory for strictly positive values of the Spalding numbers, as previously discussed in section 2.3. It is important to

highlight that, the proposed formulation of this work manages to take into account cases wherein Spalding numbers can become negative, thus invalidating the use of such correction factors. Regardless of the subsequent results, the present discussion exposes a need for more general Nusselt and Sherwood correlations specific to multi-component droplets; Particularly, correlations that are able to take into account varying states between evaporation and condensation during the lifetime of a single droplet, corresponding to outward and inward Stefan flow respectively inside the film region.

Within the solution strategy adopted for the proposed model (see section 3), the influence of the convective heat and mass transfer processes is expressed in terms of the ζ^{conv} factors as defined by both expressions in Eq. **??**. As Nusselt and Sherwood numbers are inside the ζ factors, this specific approach is labeled here *in-exp*. This specific approach contrasts for instance with the procedure described on Tonini and Cossali [6], where the authors have opted to describe the convective influence as a multiplicative factor outside of the exponential, in analogy with the single-component results obtained from Abramzon and Sirignano [9]. The effects of such an approach are also investigated here under the label *out-exp* but within the proposed model framework.

Simulation results were compared to the experimental data presented in ([35, 36]) for ethanol/water droplets with varying initial compositions represented in terms of mass fractions. In agreement with the experimental measurements, the initial droplet diameter is $d_0 = 1.2mm$, the initial droplet temperature is $T_{d,0} = 293.15K$ and the surrounding gas temperature is $T_\infty = 400K$. The droplet is exposed to a free-flow with fixed velocity $U_\infty = 2m/s$.

In Fig 10, deviations between results with and without the correction of Stefan flow effects are not expressive in all of these tested cases. However, appreciable difference is found when comparing the two different approaches used to incorporate convection effects in the proposed model. Results achieved for the *in-exp* approach delivers slightly higher evaporation rates than the *out-exp* in all simulated conditions. Such a behavior allows a slightly better agreement with the experimental data for pure components, while the opposite occurs for the liquid mixtures. Nevertheless, both approaches present a general good agreement with the experimental data.

It is important to mention that dry air has been considered in all simulation while experimental tests have been conducted with atmospheric air, which may present some humidity. The presence

of water vapor in the surrounding gas may contribute to a delay in the evaporation rate as the mass transfer potential for water (i.e. the Spalding number associated with this component - B_{H_2O}) reduces. Also, the slope of the normalized droplet surface area may change with the consideration of some relative humidity. Both aspects are observed in the results presented in sections 5-6, which may allow a better agreement with the chosen experimental data.

8. Summary and conclusions

A novel modeling approach is proposed to describe heat and mass transfer for multi-component droplets immersed in general atmosphere compositions. The model is derived from general energy and species transport equations including effects of differential diffusion in terms of the Fick's law. The derivations are described to highlight specific modeling steps as well as to clearly indicate the simplifications. Analyses have been conducted in a systematic fashion, in which the influence of different variables, properties, and formulations could be individually tested. Various scenarios were considered for the conducted analyses, which were defined by real experiments following a validation procedure or expressed in terms of artificial albeit realistic situations in order to evaluate a specific modeling aspect. As a result, a consistent and robust model could be achieved.

Investigations conducted with different binary mixtures demonstrated that the model has no restriction to run with different VLE approaches and combinations of component polarities. Within the analysis of the VLE approaches, the model has been validated for mixtures of non-polar liquids exhibiting different volatilities. Particularly, throughout the manuscript substance pairs of different volatilities prevail in order to stress the model. The comparisons of different VLE behavior associated with specific substance pairs showcase that deviations noticed in boiling point diagrams between both tested VLE approaches are reflected in typical metrics applied to analyse droplet heat and mass transfer. Particularly, alcane mixtures demonstrated to be insensitive to the considerations of the non-ideal VLE approach, while such an approach was necessary to describe the other mixture pairs.

Special attention has been paid to the representation of the droplet heat and mass transfer process at severe atmosphere conditions. Specifically, this was one of the main motivations for the derivation of the proposed model. Two kind of tests have been used to evaluate the model

robustness and the behavior of different solution strategies. The first considered comparisons with experimental data, in which methanol droplets (i.e. a hydrophilic substance with high volatility) evaporate in dry and humid air. In this framework, all of the employed models could manage to address the problem. All of them showcase a good agreement with reference experimental data and numerical predictions. Such a good agreement was more pronounced for the more severe condition, where the relative humidity is set to 100%. In view of combustion applications, an artificial test case is employed where the interaction of binary mixtures composed by reactants and products species with a freely propagating flame is emulated. Herein, the robustness of the proposed model and the limitations of other two modeling strategies could be clearly pointed out. As soon as evaporating droplets start to interact with high temperature regions which also possess high mass fractions of vapor, typical approaches fail. This is because of specific mathematical limitations. Nevertheless, the combination of the derived mathematical equations and the proposed solution strategy, the proposed model has no restrictions to address such challenges.

As the entire derivation process relies on the consideration of differential diffusion effects, a section is specifically dedicated to point out the importance of such modeling aspect for multi-component droplets. In this context, two other issues are thoroughly discussed: the calculation of multi-component and binary diffusion coefficients. Such an analysis was motivated by the perception of the inversion of the order that substances are released form the droplet surface when considering differential diffusion and non-ideal VLE approaches. As mentioned, such a behavior is not a particular characteristic of the proposed model, but it occurs with other models available in the literature as well. From the conducted analysis, it turns out that when multi-component droplet heat and mass transfer models based on differential diffusion are considered, the air humidity must be accounted for. Further investigations showcase that the choice for a specific model to address the diffusion coefficient and the consideration of differential diffusion impacts the evolution of droplet heat and mass transfer processes. The assessment of the different approaches available to address the species diffusive transport in the gas phase will be subject of future works.

Finally, convective droplet heat and mass transfer are considered for different mixtures of ethanol and water. Comparisons with experimental data successfully validated the proposed model. Altogether four modeling strategies have been tested, allowing to explore all the combinations re-

sulting from the variation of two parameters: Stefan flow correction and the embedded solution of convective effects. The correction of the Nusselt and Sherwood numbers due to the Stefan flow effects was not expressive in the simulated cases. Therefore, the more general solution demonstrated to be sufficient for the tested scenarios. However, further investigations about the possibility to include negative values of the Spalding numbers in the corresponding equations of the film theory are wanted. This is expected to improve the accuracy of the model in such cases. In contrast to the insensitivity of the Stefan flow correction, the proposed model demonstrates to be affected by the possibility to embed Nusselt and Sherwood numbers in the resulting nonlinear system of the model than their consideration *a posteriori*. Although the results given by both approaches presented a good agreement with experimental data, the embedded solution is recommended since it is more coherent with the coupled solution strategy adopted throughout this study.

9. Acknowledgements

We acknowledge the financial support from São Paulo Research Foundation (FAPESP - grant # 2017/06815-7). Support from the French Agence Nationale de la Recherche in the MIMETYC project (grant ANR-17-CE22-0003) is also acknowledged.

References

[1] R. S. Miller, K. Harstad, J. Bellan, Evaluation of equilibrium and non-equilibrium evaporation models for many-droplet gas-liquid flow simulations, International Journal of Multiphase Flow 24 (1998) 1025–1055.

[2] W. A. Sirignano, Fluid Dynamics and transport of droplets and sprays, 2nd ed., Cambridge University Press, New York, NY, 2010.

[3] F. L. Sacomano Filho, G. C. Krieger Filho, J. A. van Oijen, A. Sadiki, J. Janicka, A novel strategy to accurately represent the carrier gas properties of droplets evaporating in a combustion environment, International Journal of Heat and Mass Transfer 137 (2019) 1141–1153.

[4] G. Brenn, L. J. Deviprasath, F. Durst, C. Fink, Evaporation of acoustically levitated multi-component liquid droplets, International Journal of Heat and Mass Transfer 50 (2007) 5073–5086.

[5] V. Ebrahimian, C. Habchi, Towards a predictive evaporation model for multi-component hydrocarbon droplets at all pressure conditions, International Journal of Heat and Mass Transfer 54 (2011) 3552–3565.

[6] S. Tonini, G. E. Cossali, A novel formulation of multi-component drop evaporation models for spray applications, International Journal of Thermal Sciences 89 (2015) 245–253.

[7] P. Narasu, S. Boschmann, P. Pöschko, F. Zhao, E. Gutheil, Modeling and Simulation of Single Ethanol/Water Droplet Evaporation in Dry and Humid Air, Combustion Science and Technology 192 (2020) 1233–1252.

[8] L. Zhang, S. C. Kong, Multicomponent vaporization modeling of bio-oil and its mixtures with other fuels, Fuel 95 (2012) 471–480.

[9] B. Abramzon, W. A. Sirignano, Droplet vaporization model for spray combustion calculations, International Journal of Heat and Mass Transfer 32 (1989) 1605–1618.

[10] K. K. Kuo, Principles of combustion, 2 ed., John Wiley Sons Inc., 2005.

[11] B. Somers, The simulation of flat flames with detailed and reduced chemical models, Ph.D. thesis, Technische Universiteit Eindhoven, 1994.

[12] G. Lupo, C. Duwig, A Numerical Study of Ethanol-Water Droplet Evaporation, Journal of Engineering for Gas Turbines and Power 140 (2018) 21401.

[13] S. S. Sazhin, Advanced models of fuel droplet heating and evaporation, Progress in Energy and Combustion Science 32 (2006) 162–214.

[14] F. A. Williams, Combustion Theory, (1985), 2 ed., Addison Wesley, 1985.

[15] E. N. Fuller, P. D. Schettler, J. C. Giddings, A new method for prediction of binary gas-phase diffusion coefficients, Industrial and Engineering Chemistry 58 (1966) 18–27.

[16] E. N. Fuller, K. Ensley, J. C. Giddings, Diffusion of halogenated hydrocarbons in helium. The effect of structure on collision cross sections, Journal of Physical Chemistry 73 (1969) 3679–3685.

[17] I. V. Gnielinski, VDI-Wärmeatlas, VDI Buch, Springer Berlin Heidelberg, Berlin, Heidelberg, 2006.

[18] A. C. Santos, A. Vié, F. L. Sacomano Filho, Modeling droplet evaporation of multi-component liquid fuel, in: Proceedings of the European Combustion Meeting 2021, Neaples, Italy, 2021, p. 6.

[19] K. K. Kuo, R. Acharya, Fundamentals of turbulent and multiphase combustion, 1 ed., John Wiley Sons Inc., Hoboken, New Jersey, 2012.

[20] A. Blanc, Recherches sur les mobilités des ions dans les gaz, Journal de Physique Théorique et Appliquée 7 (1908) 825–839.

[21] S. I. Sandler, E. A. Mason, Kinetic-theory deviations from blanc's law of ion mobilities, The Journal of Chemical Physics 48 (1968) 2873–2875.

[22] T. R. Marrero, E. A. Mason, Gaseous Diffusion Coefficients, Journal of Physical and Chemical Reference Data 1 (1972) 3–118.

[23] T. P. Coffee, J. M. Heimerl, Transport algorithms for premixed, laminar steady-state flames, Combustion and Flame 43 (1981) 273–289.

[24] R. V. Mrazek, C. E. Wicks, K. N. S. Prabhu, Dependence of the Diffusion Coefficient on Composition in Binary Gaseous Systems, Journal of Chemical and Engineering Data 13 (1968) 508–510.

[25] E. A. Mason, Higher approximations for the transport properties of binary gas mixtures. I. general formulas,

The Journal of Chemical Physics 27 (1957) 75–84.

[26] E. A. Mason, Higher approximations for the transport properties of binary gas mixtures. II. Applications, The Journal of Chemical Physics 27 (1957) 782–790.

[27] B. E. Poling, J. M. Prausnitz, J. P. O'Connell, The Properties of Gases and Liquids, 5th ed., McGRAW-HILL, 2001.

[28] J. Wilms, Evaporation of Multicomponent Droplets, Phd thesis, Universität Stuttgart, 2005.

[29] E. Jones, T. Oliphant, P. Peterson, Others, SciPy: Open source scientific tools for Python, ????

[30] B. S. Garbow, K. E. Hillstrom, J. J. More, Documentation for MINPACK subroutine HYBRD: Double precision version, 1980.

[31] M. J. D. Powell, An efficient method for finding the minimum of a function of several variables without calculating derivatives, The Computer Journal 7 (1964) 155–162.

[32] C. K. Law, T. Y. Xiong, C. Wang, Alcohol droplet vaporization in humid air, International Journal of Heat and Mass Transfer 30 (1987) 1435–1443.

[33] C. Chauveau, M. Birouk, I. Gökalp, An analysis of the d2-law departure during droplet evaporation in microgravity, International Journal of Multiphase Flow 37 (2011) 252–259.

[34] A. Bader, P. Keller, C. Hasse, The influence of non-ideal vapor-liquid equilibrium on the evaporation of ethanol/iso-octane droplets, International Journal of Heat and Mass Transfer 64 (2013) 547–558.

[35] L. Ma, X.-q. Qiu, J. Wang, Z.-w. Zheng, Z.-y. Yi, H.-q. Yang, Experimental research on single droplet evaporation factors, Modern Chemical Industry 33 (2013) 103–106.

[36] L. Ma, Y. Chou, X. Cui, Z. Zheng, Research on double-component droplets evaporation properties, Industrial Heating 43 (2014) 13–16.

[37] M. Lapuerta, J. P. Hernández, J. R. Agudelo, An equation for the estimation of alcohol-air diffusion coefficients for modelling evaporation losses in fuel systems, Applied Thermal Engineering 73 (2014) 539–548.

[38] E. A. Mason, L. Monchick, Transport properties of polar-gas mixtures, The Journal of Chemical Physics 36 (1962) 2746–2757.

[39] C. C. Wen, C. H. Tu, Vapor-liquid equilibria for binary and ternary mixtures of ethanol, 2-butanone, and 2,2,4-trimethylpentane at 101.3 kPa, Fluid Phase Equilibria 258 (2007) 131–139.

[40] Y. Peng, X. Lu, B. Liu, J. Zhu, Separation of azeotropic mixtures (ethanol and water) enhanced by deep eutectic solvents, Fluid Phase Equilibria 448 (2017) 128–134.

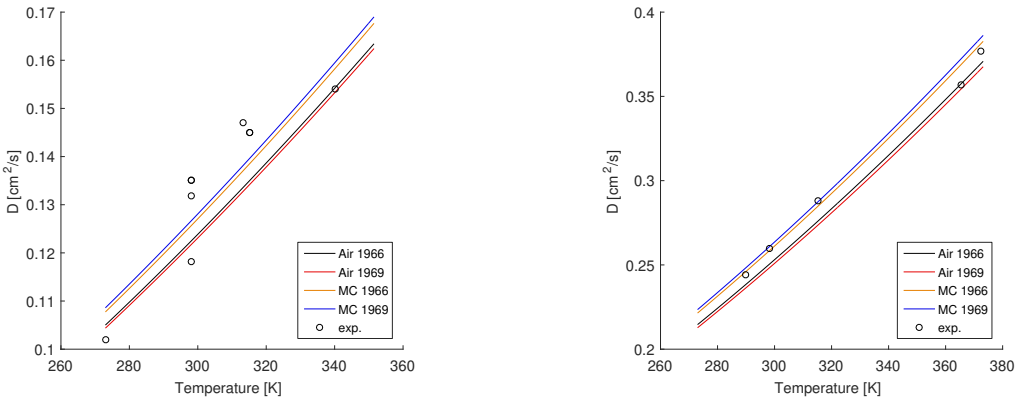

(a) ethanol in air

(b) water in air

Figure 2: Values of the diffusion coefficient D for ethanol (a) and water (b) in air computed with different approaches at different temperatures and at atmospheric pressure. Lines refers to computed values, while marks to experimental data. Experimental data for ethanol (a) are extracted from [37] and [38], while for water all data are obtained from [38].

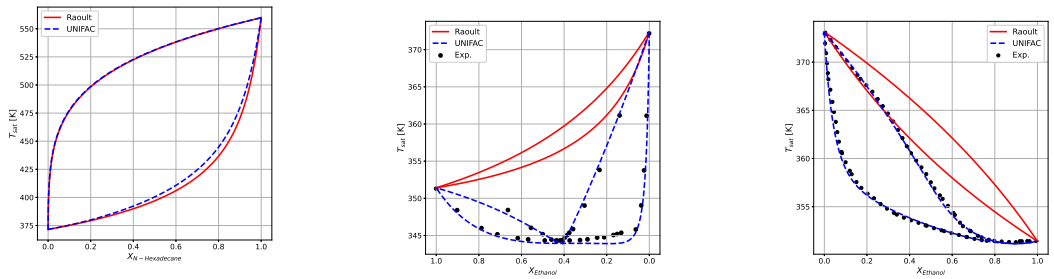

(a) n-hexadecane/n-heptane (NN)

(b) ethanol/iso-octane (PN)

(c) ethanol/water (PP)

Figure 3: Boiling-point diagrams for three mixtures with different polarity behaviors at 1 atm. The experimental data presented in (b) and (c) are extracted from [39] and [40], respectively.

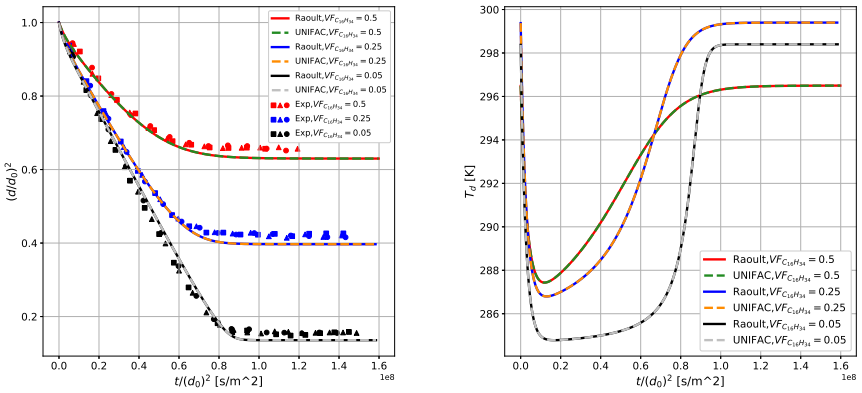

Figure 4: Comparison of VLE approaches through normalized droplet surface and temperature evolution for a n-hexadecane/n-heptane droplet with initial diameter $d_0 = 50\mu m$. Temperatures are $T_{d,0} = T_\infty = 296.5K$ for the initial composition $VF_{C_{16}H_{34}} = 0.5$, $T_{d,0} = T_\infty = 299.4K$ for the initial composition $VF_{C_{16}H_{34}} = 0.25$ and $T_{d,0} = T_\infty = 298.4K$ for the initial composition $VF_{C_{16}H_{34}} = 0.05$. Experimental data extracted from [28]

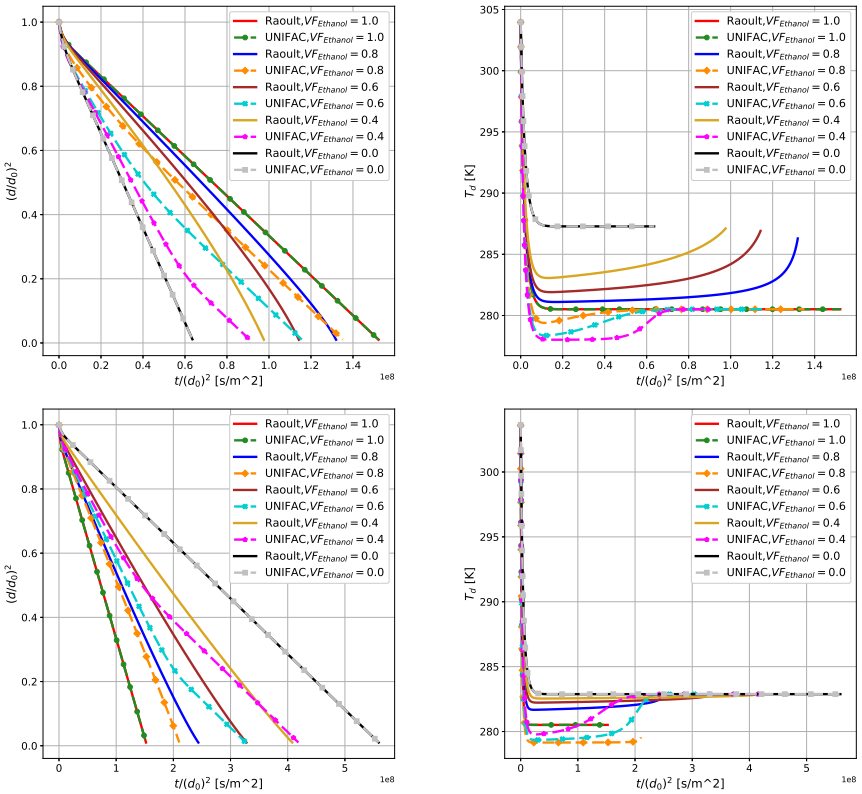

Figure 5: Comparison of VLE approaches through normalized droplet surface and temperature evolution for a ethanol/iso-octane (top) and ethanol/water (bototm) droplets with initial diameter $d_0 = 50\mu m$, initial temperature $T_{d,0} = 304K$, surrounding gaseous temperature $T_\infty = 304K$ and varying initial compositions.

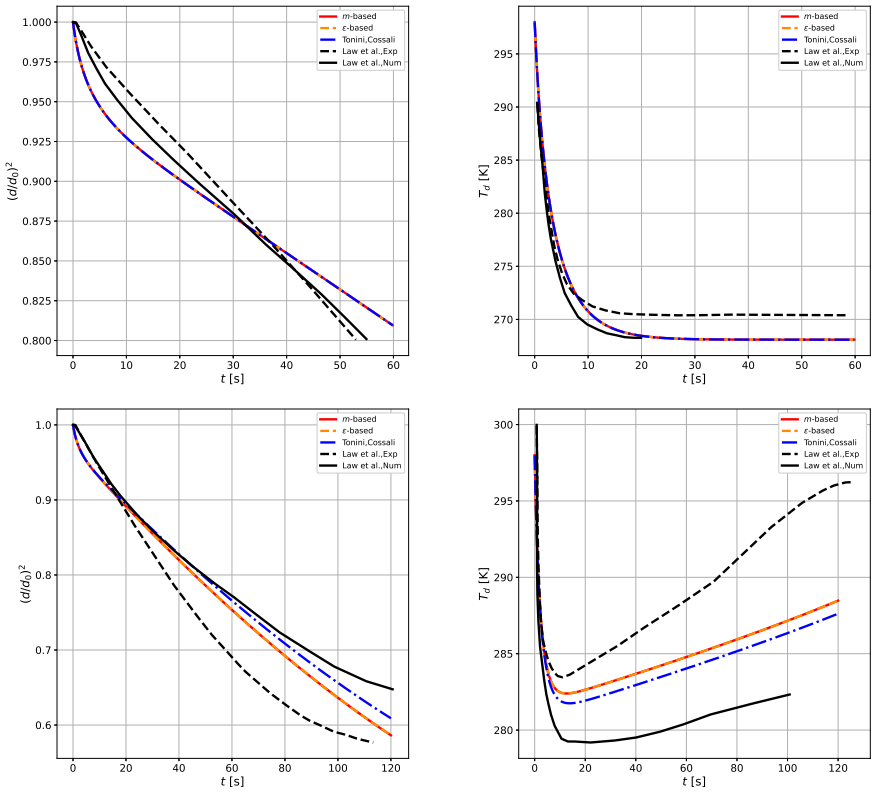

Figure 6: Comparison of modeling approaches through normalized droplet surface and temperature evolution for a pure Methanol droplet with relative air humidity *phi* = 0.0 (top) and ϕ = 1.0 (bottom)

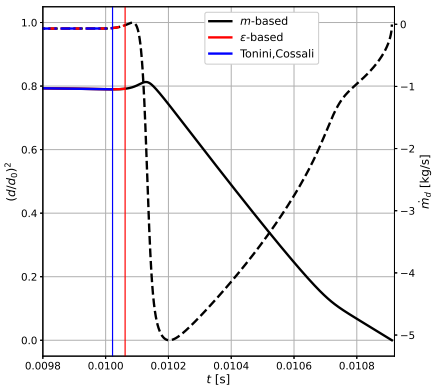

Figure 7: Normalized droplet surface area (continuous lines) and evaporation rate (dashed lines) for a pure Methanol droplet of initial diameter $d_0 = 20\mu m$ and temperature $T_{d,0} = 300K$ moving through a region of length $L_0 = 0.5cm$ $T_\infty = 300K$ until meeting a flame-front of thickness $L_{flame} = 0.1mm$ wherein both the temperature and the water composition vary following a hyperbolic tangent profile from $T_\infty = 300K$ to approximately $T_\infty = 2000K$ and $Y_{\infty,Wat} = 0$ to approximately $Y_{\infty,Wat} = 0.15$ respectively

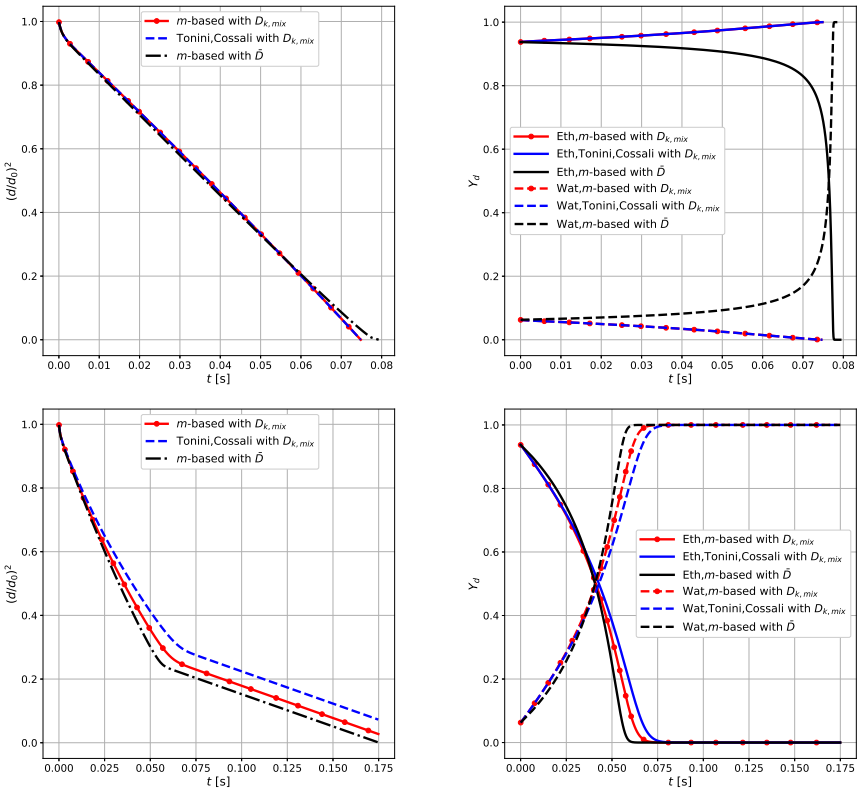

Figure 8: Normalized droplet surface and internal composition for a $VF = 0.95$ ethanol/water droplet of initial diameter $d_0 = 20\mu m$ and temperature $T_{d,0} = 300K$ with surrounding gaseous temperature $T_\infty = 300K$ and relative humidity of $\phi = 0.0$ (top) and $\phi = 0.4$ (bottom)

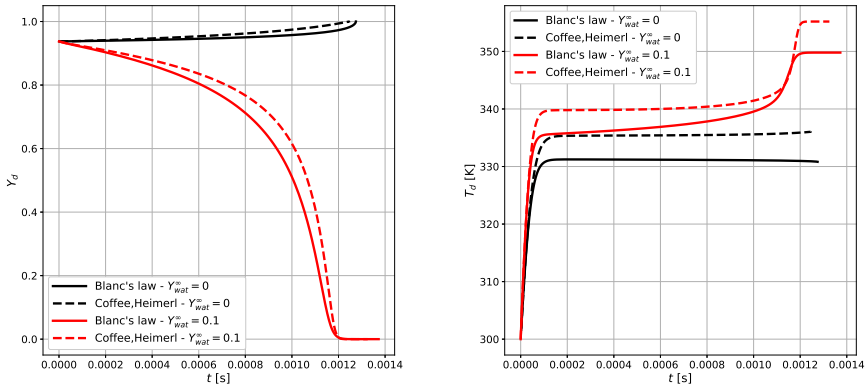

Figure 9: Ethanol composition inside droplet and droplet temperature for a $VF = 0.95$ ethanol/water droplet of initial diameter $d_0 = 20\mu m$ and temperature $T_{d,0} = 300K$ with surrounding gaseous temperature $T_\infty = 1500K$ and water mass fraction at infinity $Y^{\infty}_{wat} = 0.0$ and $Y^{\infty}_{wat} = 0.1$

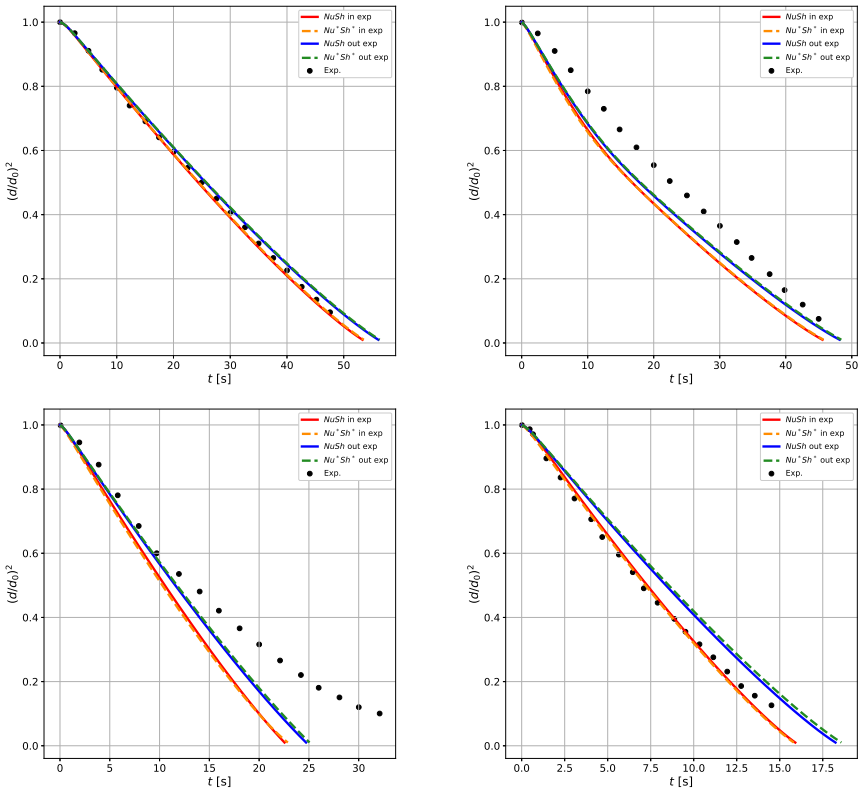

Figure 10: Normalized droplet surface and temperature for varying initial compositions ($VF_{Eth} = 0$, $VF_{Eth} = 0.25$, $VF_{Eth} = 0.75$, $VF_{Eth} = 1.0$ left-to-right, top-to-bottom) of a ethanol/water droplet of initial diameter $d_0 = 1.2mm$ and temperature $T_{d,0} = 293.15K$ with surrounding gaseous temperature $T_\infty = 400K$